IET Microwaves, Antennas & Propagation

Research Article

IET Journals
The Institution of Engineering and Technology

Design of multi-standard single/tri/quint-wideband asymmetric stepped-impedance resonator filters with adjustable TZs

ISSN 1751-8725
Received on 4th October 2018
Revised 23rd April 2019
Accepted on 1st May 2019
E-First on 4th June 2019
doi: 10.1049/iet-map.2018.5863
www.ietdl.org

Yasir I.A. Al-Yasir[1], Yuxiang Tu[1], Mustafa S. Bakr[2], Naser Ojaroudi Parchin[1], Abdalfettah S. Asharaa[1], Widad A. Mshwat[1], Raed A. Abd-Alhameed[1] ✉, James M. Noras[1]

[1]*School of Electrical Engineering & Computer Science, Bradford University, Bradford, UK*
[2]*Institute of Microwave and Photonics, University of Leeds, Leeds, UK*
✉ *E-mail: r.a.a.abd@bradford.ac.uk*

Abstract: This study presents an original asymmetric stepped-impedance resonator filter combined with meander coupled-line structures and enabling the realisation of finite transmission zeros (TZs) and the implementation of multi-band bandpass filters. The meander coupled sections (MCSs) tune the TZs and resonant frequencies: with higher-order spurious frequencies cancelled by the TZs, a single wideband with wide stopband from 1.18 to 1.84 GHz is possible. Furthermore, by positioning the finite TZs between the high-order spurious frequencies and adjusting the coupling strength between resonators, a quint-wideband filter can be realised, with centre frequencies of 1.19, 4.29, 5.43, 6.97, 9.9 GHz and fractional bandwidths of 31.9, 15.4, 15.8, 4.3, 39.2%, respectively. More importantly, two filters with single/quad-wideband performance can be realised by tuning the parameters of the MCS, and therefore they can be designed separately by using only one original structure. The triple-wideband filter is realised with the help of the asymmetric parallel uncoupled microstrip section. These filter structures enjoy the advantage of single/multi-band versatility, structure reusability and simplicity. The good in-band and out-of-band performance, low loss and simple structure of the proposed single/tri/quint-wideband filters make them very promising for applications in future multi-standard wireless communication.

1 Introduction

With the growth of multi-service wireless communication networks, microwave components and systems that support various modern communication standards have become increasingly important. In particular, the multi-standard bandpass filter (BPF) design demands high performance with compact size for enhanced system functionality. Such filters are usually required to be capable of covering the operating bands of the global positioning system (GPS: 1227.6 MHz, 1.57 GHz), global system for mobile communication (GSM: 1800/1900 MHz etc.), the universal mobile telecommunications system (UMTS: 1710–1880/1850–1990/1920–2170 MHz etc.) and IEEE 802.11a (5 GHz). Suitable filters need to have relative high fractional bandwidth (FBW), low insertion loss and low return loss. However, the need for filters to be physically small means that many designs are inadequate, failing to cover the required frequency bands due to their narrow BW and low FBW [1–5]. Increasing the size or requiring extra structures such as via holes means that the resulting filters are too complicated for fabrication and are difficult to integrate within multi-standard wireless communication systems [6–16]. Critically, most proposed filter structures [1, 17] can only realise single-band or multi-band performance by utilising various different structures, which results in lower reusability, higher complexity and higher cost. Compared to the traditional stepped-impedance resonator (SIR) with two step discontinuities, the asymmetric SIR (ASIR) has only one discontinuity but retains controllability of spurious modes. Thus, it combines the advantages of compact size, lower loss and strong design feasibility, particularly in high-order BPFs such as dual band [17], triple band and quad band [18], because of its inherent higher-order resonant modes. Published coupled-line ASIR structures can be classified into two types: anti-parallel-coupled (APC) or parallel-coupled ASIRs. The APC-ASIR, consisting of two ASIR units with their high- and/or low-impedance lines anti-coupled with each other, is usually folded at its open end. In [17], the high-impedance lines of two ASIRs are bent and coupled with each other to form a signal transmission route, and the first spurious frequency is utilised to form the second operating band [19]. Since the frequency response characteristic of the APC line is determined by the frequency response characteristic of the ASIR, the APC-ASIR frequency response is easy to calculate. However, the BW characteristic of the APC-ASIR structure [4, 17], as with the multi-stage-coupled ASIR structure [18, 20], is usually limited within the narrowband characteristic range and is not suitable to realise wideband performance. Therefore, this approach cannot fully meet the multi-service requirement of current wireless communication.

The second type, the parallel-coupled ASIR structure, has ASIRs with their high-impedance lines parallel coupled with each other: this is also called the skew-symmetrical ASIR (SS-ASIR) coupled pair. Using this kind of structure, characteristics of frequency response performance such as BW, return loss and insertion loss can be greatly improved at some frequency points, without changing or degrading the performance generally. This facilitates designs with wide BW and large FBW, different from the narrowband characteristic exhibited in traditional ASIR structures [4, 17, 19]. However, until now, the proposed ASIR structures could only realise narrowband characteristics [4, 17–20] or dual/quad-wideband characteristics, with the disadvantages of uncontrollable or limited transmission zeros (TZs) seriously restricting their application range.

In this work, we propose novel multi-standard single/tri/quint-wideband ASIR filters to solve the problems mentioned above. The proposed filters are capable of generating wide operating bands which effectively cover the GPS/GSM/UMTS/IEEE 802.11a application in wireless communication systems including the GPS (1227 MHz, 1.57 GHz), the GSM1800/1900 (1710–1880 MHz, 1850–1990 MHz) and the UMTS (1920–2170 MHz). These filters share the same original structure, with their performance optimised by tuning relative TZs. Therefore, the design enjoys advantages of versatility and simplicity, with reduced design complexity and cost. Good agreement is observed between the simulated and measured results. Although a slight difference at the higher frequencies can be observed, this mismatch can be explained by an error in the manufacturing process or/and a variation in the material properties.

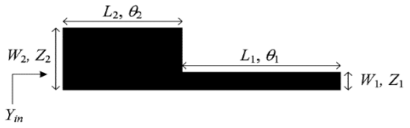

Fig. 1 *Structure of an ASIR*

Table 1 Transformation relationship of in-band performance of the SS-ASIR coupled pair and ASIR unit, when α ranges from 0.4 to 0.7

α	Fundamental frequency f_0	First spurious frequency f_{s1}	Second spurious frequency f_{s2}	Third spurious frequency f_{s3}	Fourth spurious frequency f_{s4}
0.4	improved	no significant change (NC)/ degradation (DE)	improved	NC/DE	improved
0.42	improved	NC/DE	improved	NC/DE	improved
0.5	improved	NC/DE	improved	NC/DE	improved
0.55	improved	NC/DE	NC/DE	improved	NC/DE
0.57	improved	NC/DE	improved	improved	NC/DE
0.6	improved	improved	NC/DE	improved	NC/DE
0.65	improved	improved	NC/DE	NC/DE	improved
0.7	improved	improved	NC/DE	NC/DE	NC/DE

'Improved' means significantly enhanced performance at relative frequency and 'NC/DE' means no significant change or degradation of performance at relative frequency point.

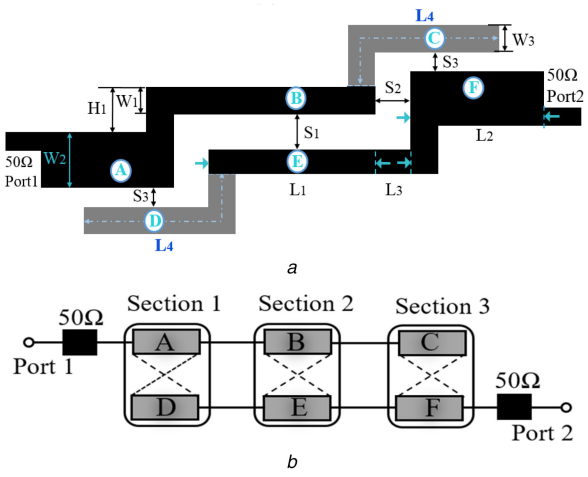

Fig. 2 *SS-ASIR coupled pair with MCS*

(a) Schematic diagram, ***(b)*** Equivalent circuit and coupling routing schemes for the proposed filter

In fact, the fabrication tolerances, as well as the subminiature version A connectors and the calibration errors may have led to the discrepancies between the simulated and measured results in the upper stopband.

To the best of the authors' knowledge, the proposed ASIR filters realise for the first time a single-wideband filter with wide stopband and a quint-wideband filter at the same time, by using the same structure as in recently proposed single/multi-band filters [1–21]. Moreover, a quint-wideband filter can be realised with large FBWs for all operating bands in comparison with [11–13].

The proposed filters use the capacitive coupling of only two miniaturised ASIRs to realise single/tri/quint-wideband operation without adding any extra structure such as via holes or defected ground structure, which is also novel for single/multi-wideband filters [1–21].

2 In-band performance enhancement method and TZs adjusting method

2.1 In-band performance enhancement method

To enhance the filter in-band performance, the SS-ASIR structure is used. In the design, the frequency response transformation relationship between the parallel-coupled ASIR and the ASIR unit needs to be considered so as to enhance the performance in the desired frequency band. In Fig. 1, the electrical length ratio α equals $\theta_2/(\theta_2+\theta_1)$, where θ_1 and θ_2 are the electrical lengths of sections L_2 and L_1 in the ASIR, respectively. The characteristic impedance ratio K equals Z_2/Z_1, where Z_1 and Z_2 are the characteristic impedances of sections L_2 and L_1 in the ASIR, respectively. The transformation relationship table is shown in Table 1.

2.2 TZs generating and tuning method in the SS-ASIR structure

Fig. 2*a* shows the topological structure of the SS-ASIR coupled pair rearranged by the meander coupled lines (MCLs) to form the (SSMCL-ASIR), which is shown as the grey part with width W_3 and length L_4. The meander coupled section (MCS) is added at the open end of the high-impedance coupled line in the SS-ASIR coupled pair. Fig. 2*b* shows the equivalent circuit and the coupling routeing scheme of Fig. 2*a*.

The main signal is coupled to the two half-wavelength resonators at the same time, providing the two main paths between the two ports. Each ASIR resonator of the filter consists of three cascaded sections. The A–B–C sections form the first resonator (ASIR 1) and D–E–F sections form the second resonator (ASIR 2). In addition to the usual single coupling route of B–E for the main coupled transmission lines represented by Section 2, two extra coupling routes, namely A–D for Section 1 and C–F for Section 3, are created by the adoption of MCLs. This multi-path coupling routeing scheme of the modified SSMCL-ASIR filter is shown in Fig. 2*b*. Owing to the multi-path coupling routing, more TZs are

created, which are utilised to suppress high-order spurious frequencies or to help facilitate multi-band performance.

Since the harmonic frequency performance would degrade when using the SS-ASIR structure, first spurious frequency (f_{si}) cannot be conveniently deduced by simply analysing $Y_{in} = 0$ in the ASIR unit. However, TZ frequency (f_{zi}) can still be obtained by setting $Z_{ine} = Z_{ino}$, where Z_{ine} and Z_{ino} are the input impedances for the even- and odd-mode equivalent circuits, respectively. The necessary and sufficient conditions for $Z_{ine} = Z_{ino}$ is $S_{21} = 0$ and the equivalent ***Y***-parameter matrix of the even- or odd-mode equivalent circuit of the proposed structure can be expressed as (see (1)) , where θ_{01} and $\theta_4$are the electrical lengths of the original coupled line and of the MCS, respectively. Z_{0even} and Z_{0odd} are the even- and odd-mode characteristic impedances for each coupled section, respectively.

Since all elements of the normalised ***Y***-parameters in (1) are purely imaginary, S_{21} of this coupled line can be expressed as

$$S_{21} = -\frac{2\mathrm{jIm}\{y_{12}\}}{1-\mathrm{Im}\{y_{11}\}^2+\mathrm{Im}\{y_{12}\}^2+2\mathrm{jIm}\{y_{11}\}} \tag{2}$$

Substituting from (1) into (2) gives the equation below:

(see (3))

where (see equation below). According to (3), there are three cases leading to $S_{21} = 0$. The first case is $Z_{0even} = Z_{0odd}$. The MCS of length L_4 can be seen as a shifted coupled-line (SCL) structure which can suppress the spurious peak by compensating even-mode and odd-mode phase velocities. When the coupled-line insertion loss is zero, the coupled length for the SCL/MCL can be obtained from the following equation:

$$\frac{Z_{0even}}{Z_{0odd}} = \frac{\sin\beta_{even}L_4}{\sin\beta_{odd}L_4} \tag{4}$$

when $Z_{0even} = Z_{0odd}$, $\sin\beta_{even}L_4 = \sin\beta_{odd}L_4$. Also

$$\beta_{even}L_4 = \beta_{odd}L_4 + k_1\pi \quad (k_1 = 0, 1, 2, 3, \ldots) \tag{5}$$

In this design, $0 < \beta_{even}L_4 < \pi$ and $0 < \beta_{odd}L_4 < \pi$, thus $k_1 = 0$ and $\beta_{even} = \beta_{odd}$. Since $v_{p,even} = \omega_{even}/\beta_{even}$ and $v_{p,odd} = \omega_{odd}/\beta_{odd}$, then $v_{p,\,even} = v_{p,odd}$ when $\omega_{even} = \omega_{odd}$. Here, $v_{p,\,even}$, ω_{even} and β_{even} are even-mode phase velocity, angular frequency and phase constant, respectively. $v_{p,\,odd}$, ω_{odd} and β_{odd} mean odd-mode phase velocity, angular frequency and phase constant, respectively. When the even-mode and odd-mode phase velocities are equal, TZs are generated and the spurious peak can be suppressed. Fig. 3 compares frequency responses with and without an SCL/MCS. As shown in this figure, without an SCL/MCS the unsuppressed spurious frequencies f_{s2} and f_{s3} exist and seriously limit the stopband BW. With an SCL/MCS, f_{s2} and f_{s3} are effectively suppressed and a wide stopband is generated. Moreover, because the whole coupled-line length is extended by the SCL/MCS structure, both the fundamental and spurious frequencies are shifted to lower frequencies.

The second case is $\sin(\theta_{01} + \theta_4) = 0$, namely

$$\theta_{01} + \theta_4 = k\pi \quad (k = 1, 2, 3, \ldots). \tag{6}$$

When $k = 1$ for the shortest whole coupled-line electrical length, $\theta_{01} + \theta_4 = \pi$, and the corresponding coupled-line physical length can be calculated as

$$L_1 + L_4 = \frac{\lambda_g}{2} \tag{7}$$

where L_1 and L_4 are the physical lengths corresponding to θ_{01} and θ_4, respectively. The third case is $u = 0$ and $v = 0$. When $u = 0$

$$\theta_{01} + \theta_4 = 2\sin^{-1}\sqrt{\frac{Z_{0even}Z_{0odd}}{(Z_{0even}+Z_{0odd})^2+4}} \tag{8}$$

Equation (8) shows the relationship between the whole coupled-line electrical length and odd-mode and even-mode impedances of the whole coupled lines. When $v = 0$, $\sin[2(\theta_{01} + \theta_4)] = 0$

$$\theta_{01} + \theta_4 = \frac{k\pi}{2} \quad (k = 1, 2, 3, \ldots). \tag{9}$$

In general, the shortest whole coupled-line electrical length to realise $S_{21} = 0$ can be got in the third case when k is equal to 1 and $\theta_{01} + \theta_4 = \pi/2$. The corresponding coupled-line physical length can then be calculated as

$$L_1 + L_4 = \frac{\lambda_g}{4} \tag{10}$$

3 Single-wideband ASIR filter design

According to the frequency response transformation relationship discussed in Section 2, the electrical length ratio α is 0.57 when L_2 is 11.4 mm, thus setting the fundamental frequency to around 1.51

$$\begin{bmatrix} y_{11} & y_{12} \\ y_{21} & y_{22} \end{bmatrix} = \frac{1}{B}\begin{bmatrix} -\mathrm{j}\dfrac{Z_{0even}+Z_{0odd}}{2}\cot(\theta_{01}+\theta_4) & \mathrm{j}\dfrac{Z_{0even}-Z_{0odd}}{2}\csc(\theta_{01}+\theta_4) \\ \mathrm{j}\dfrac{Z_{0even}-Z_{0odd}}{2}\csc(\theta_{01}+\theta_4) & -\mathrm{j}\dfrac{Z_{0even}+Z_{0odd}}{2}\cot(\theta_{01}+\theta_4) \end{bmatrix} \tag{1}$$

$$B = -Z_{0even}Z_{0odd}\cot^2(\theta_{01}+\theta_4) + \frac{(Z_{0even}-Z_{0odd})^2}{4}$$

$$\begin{aligned} S_{21} &= -\frac{4\mathrm{j}(Z_{0even}-Z_{0odd})\dfrac{1}{\sin(\theta_{01}+\theta_4)}}{4-(Z_{0even}+Z_{0odd})^2\dfrac{\cos^2(\theta_{01}+\theta_4)}{\sin^2(\theta_{01}+\theta_4)}+(Z_{0even}-Z_{0odd})^2\dfrac{1}{\sin^2(\theta_{01}+\theta_4)}+4\mathrm{j}(Z_{0even}+Z_{0odd})\dfrac{\cos(\theta_{01}+\theta_4)}{\sin(\theta_{01}+\theta_4)}} \\ &= -\frac{4\mathrm{j}(Z_{0even}-Z_{0odd})\sin(\theta_{01}+\theta_4)}{u+\mathrm{j}v} \\ &= \frac{4\mathrm{j}(Z_{0even}-Z_{0odd})\sin(\theta_{01}+\theta_4)}{v^2-u^2}(u+\mathrm{j}v) \end{aligned} \tag{3}$$

$$\begin{cases} u = 4\sin^2(\theta_{01}+\theta_4) - (Z_{0even}+Z_{0odd})^2\cos^2(\theta_{01}+\theta_4) + (Z_{0even}-Z_{0odd})^2 \\ v = 4(Z_{0even}+Z_{0odd})\cos(\theta_{01}+\theta_4)\sin(\theta_{01}+\theta_4) \end{cases}$$

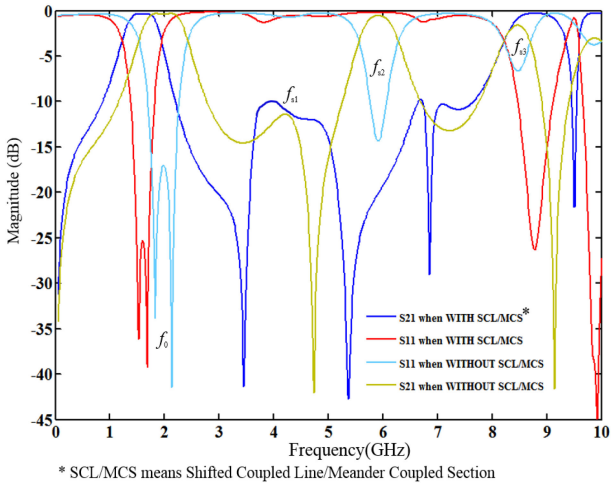

Fig. 3 *Frequency response comparison with and without SCL/MCS*

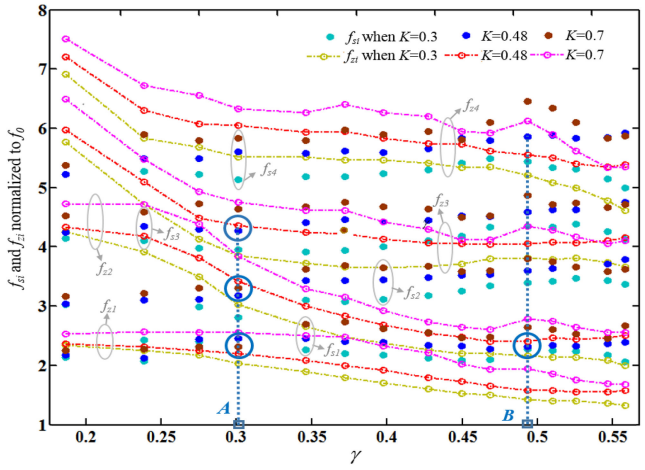

Fig. 4 *f_{si} and f_{zi} Normalised to f0 versus γ for different values of K in SSMCL-ASIR structure*

GHz. The in-band performance of the first band such as the insertion loss and return loss is improved when the impedance ratio K is 0.48.

The dimensions of the resonator are chosen as follows: $L_1 = 14$ mm, $L_2 = 11.4$ mm, $L_1 + L_3 = 15.2$ mm, $W_1 = 0.4$ mm and $W_2 = 1.6$ mm. Through the design procedure for the coupled resonator circuits, the gaps of the whole coupled lines in Fig. 2 are determined as $S_1 = 1.2$ mm, $S_2 = 0.2$ mm and $S_3 = 0.4$ mm. The use of different gaps adds more design freedom for the filter. For simplicity of design, the meander coupled structure width W_3 is made 0.4 mm, which is the same as the width of coupled lines.

Since the fundamental frequency is 1.51 GHz, the relative λ_g can be calculated as 77.4 mm. Therefore, the value of $(L_1 + L_4)$ is about 19.4 mm. L_1 is 14 mm, so L_4 is set at around 5.4 mm. Although sections L_3 and H_1 would become coupled parts after adding the MCS, the effects are small. The influence of these sections to the overall performance can, therefore, be disregarded; their coupling is much weaker than that involving sections L_1 and section L_4.

To further analyse the influence of the MCS on the resonance frequency f_{sm} and TZ frequencies f_{zn}, the normalised f_{sm} ($m = 1, 2, 3, 4$) and normalised f_{zn} ($n = 1, 2, 3, 4$) versus γ for different values of K are illustrated in Fig. 4, where γ is the electrical length ratio between the MCS θ_4 and whole coupled line $(\theta_1 + \theta_4)$ and $\gamma = \theta_4/(\theta_1 + \theta_4)$.

It can be seen in Fig. 4 that for a fixed K value, the normalised f_{zn} ($n = 1, 2, 3, 4$) decline continuously and the normalised f_{sm} ($m = 1, 2, 3, 4$) follows an approximate sinusoidal curve when γ ranges from 0.17 to 0.58. Larger K values result in larger normalised f_{zi} and larger normalised f_{si} for a fixed γ value. Since the normalised f_{si} follows an approximate sinusoidal curve and f_{zi} follows a decreasing curve, they can intersect at a certain γ value. As illustrated, at point A, when $K = 0.30$, f_{z1} approaches f_{s1}, f_{z2} approaches f_{s2} and f_{z3} approaches f_{s3}. That means the first spurious frequency, the second spurious frequency and the third spurious frequency are suppressed successfully when $K = 0.30$. The corresponding L_4 can be calculated as 5.7 mm, which is close to the theoretical value.

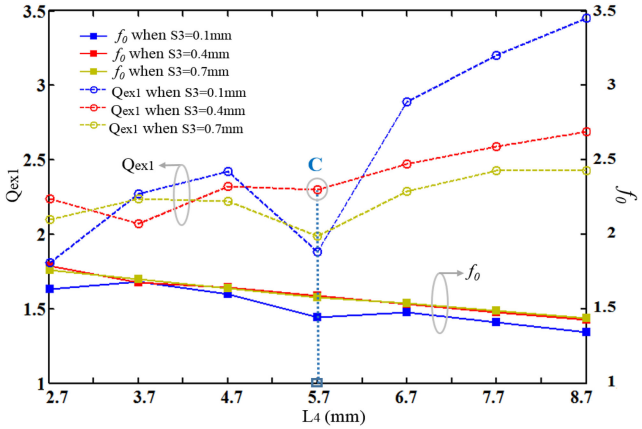

Fig. 5 *External quality factor (Q_{ex1}) with L_4*

The coupling matrix discussed in [22] will not be discussed in this paper because of its wideband limitation [22, 23]. The coupling between two ASIRs can be represented by a J-inverter susceptance $J_{1,2}$, where subscripts 1 and 2 denote the first and second passbands. A larger value of $J_{1,2}$ means a stronger coupling strength between two ASIRs. The external quality factor $Q_{ex1,2}$ and the normalised J-inverter susceptance $\overline{J_{1,2}}$ can be related by [23] as

$$Q_{ex1,2} = \frac{\pi}{2\overline{J_{1,2}}^2} \tag{11}$$

The external quality factor $Q_{ex1,2}$ can be further extracted by

$$Q_{ex1,2} = \frac{f_{c1,2}}{\Delta_{1,2}} = \frac{f_{c1,2}}{\Delta_{(\pm\frac{\pi}{2})1,2}} \tag{12}$$

where $f_{c1,2}$, $\Delta_{1,2}$, $\Delta_{(\pm\frac{\pi}{2})1,2}$ represent the central frequency (CF), −3 dB BWs and the frequency BW of phase curve changing $\pm\pi/2$ with respect to $f_{c1,2}$, respectively. From (11) and (12), $\overline{J_{1,2}}$ can be calculated by substituting the extracted $Q_{ex1,2}$ into (11).

The two transmission lines are represented as two half-wavelength microstrip line resonators. In the filter, the total length (L) of the resonator is equal to $L_1 + L_2 + L_3 + L_4 = 32.3$ mm. So the guided wavelength of the resonator can be calculated as $\lambda_g = 64.6$ mm. Since $W/h < 1$, then the effective dielectric constant can be calculated as

$$\varepsilon_{re} = \frac{\varepsilon_r + 1}{2} + \frac{\varepsilon_{re} - 1}{2}\left\{(1 + 12(W/h))^{-0.5} + 0.04(1 - (W/h))^2\right\} = 7$$

Then, the resonant frequency can be calculated as follows:

$$f_0(\text{GHz}) = \frac{300}{\lambda_g(\text{mm}) \times \sqrt{\varepsilon_{re}}} = 1.8\,\text{GHz}$$

Fig. 5 plots f_0 and external quality factor (Q_{ex1}) versus L_4 for different gap S_3 values in an SSMCL-ASIR single-band-type filter. In Fig. 5, when L_4 ranges from 2.7 to 8.7 mm, the fundamental frequency f_0 decreases continuously while Q_{ex1} increases, in

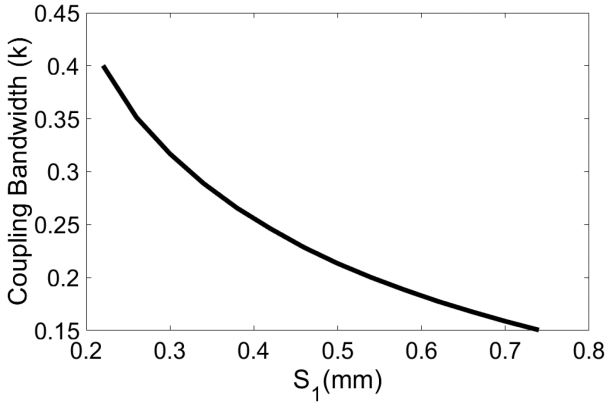

Fig. 6 *Coupling BW (K) with the gap size (S_1)*

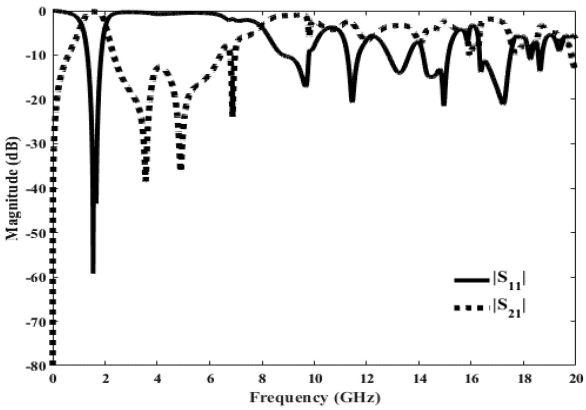

Fig. 7 *Up to 20 GHz frequency response for the proposed ASIRs*

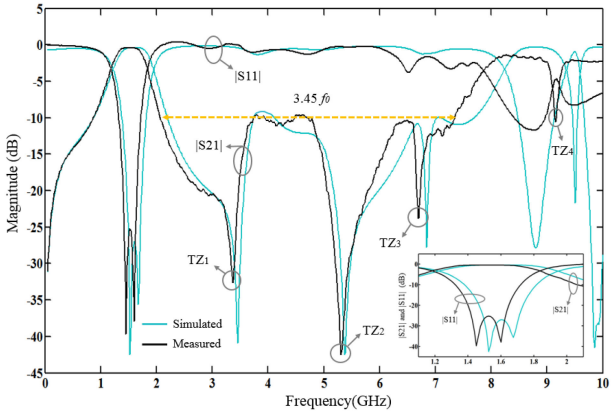

Fig. 8 *Simulated, measured results and zoom in-band performance of single-wideband-type SSMCL-ASIRs*

general, for a fixed S_3 value. Here, f_0 increases when S_3 ranges from 0.1 to 0.4 mm and does not change much when S_3 ranges from 0.4 to 0.7 mm, and Q_{ex1} decreases continuously when S_3 ranges from 0.1 to 0.7 mm, in general. Moreover, it is noted that there are two notches when $S_3 = 0.1$ and 0.7 mm, which means the BW is maximum when $L_4 = 5.7$ mm within the range of L_4 from 3.7 to 8.7 mm.

By comprehensively considering the BW, resonant frequency location and out-of-band spurious frequency suppression performance S_3 is set to 0.4 mm, which is shown as point C in Fig. 5.

Fig. 6 plots the variation of coupling BW as a function of the gap size (S_1) between the two resonators. It can be noted that increasing the gap between the resonators reduces the coupling BW of the designed filter and vice versa. Given the required electrical length ratio α, coupling coefficients and external quality factor for the proposed filter, one may determine the proper specifications based on Figs. 1, 5, 6 and Table 1. The proposed filters, fabricated

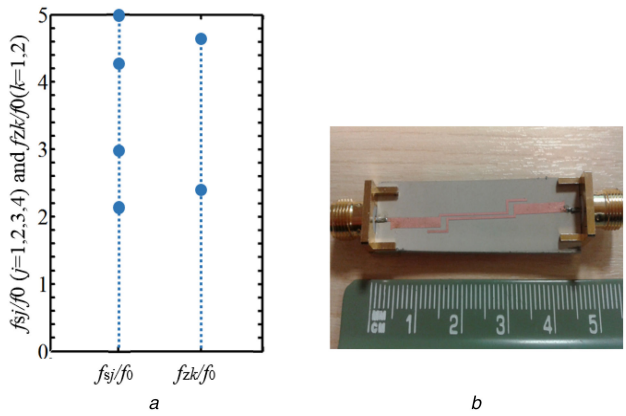

Fig. 9 *Wide stopband*
(a) f_{sj} and f_{zk} Locations of the traditional structure, ***(b)*** Single-wideband-type SSMCL-ASIR filter

on an RO3210 substrate with a relative dielectric of 10.2 and dielectric loss tangent 0.003, have been measured using an HP8510 vector network analyser. Wideband frequency response for the proposed ASIRs is shown in Fig. 7. The simulated *S*-parameters measured *S*-parameters and zoom in-band performance of the designed single-wideband SSMCL-ASIRs are plotted in Fig. 8.

Good agreement can be observed between the simulated and measured results and the slight discrepancies are attributed to loss and fabrication errors. It can be seen that the single-wideband filter is realised with very low insertion isolation of only 0.36 dB at CF and return loss of better than 25.5 dB.

The pass band ranges from 1.18 to 1.84 GHz with CF 1.51 GHz, BW 660 MHz and FBW 43.7%. It can be applied in the GPS (GPS: frequency band centred at 1.57 GHz), GSM communication (GSM: 1800 MHz) and universal mobile telecommunication system (UMTS: 1710–1880 MHz etc.).

Since the adjustable TZs $f_{z1} = 3.38$ GHz, $f_{z2} = 5.31$ GHz and $f_{z3} = 6.71$ GHz are close to the spurious frequencies, a wide stopband ranging from 2.1 to 7.32 GHz is realised, as shown in Fig. 9*a*. Normalised resonant frequencies f_{sj} and TZ frequencies f_{zk} locations with the traditional structure are plotted in Fig. 9*a* for comparison. Fig. 9*b* shows a photograph of the single-wideband-type SSMCL-ASIR and its performance comparison with other single-band BPFs are shown in Table 2.

The proposed structure can be extended to higher-order modes by cascading the basic building block, i.e. the ASIR resonator. As an example, a three-pole bandpass is shown in Fig. 10 with two TZs on the high side, giving an improved out-of-band performance. Higher-order filters are obtainable by cascading more building blocks.

4 Quint-wideband ASIR filter design

As stated above, TZs can be created and utilised to give a multi-band frequency response. The variations of S_{11} and S_{21} for different

Table 2 Performance comparison with the proposed single-band BPF

Reference	CF, GHz	−3 dB, FBW	insertion loss (IL), dB	Stopband suppression	Number, T_{zs}	Size	Single/multi-band versatilities
[5]	2.4	8.4%	2.06	up to 5.5 f_0	2	$0.36\lambda_g \times 0.13\lambda_g$	no
[9]	1.45	57.9%	1	1.45 f_0–3.35 f_0	4	$0.664\lambda_g \times 0.133\lambda_g$	no
[10]	5	40%	0.7	1.26 f_0–3.52 f_0	2	$0.294\lambda_g \times 0.162\lambda_g$	no
[21]	2.4	—	3.3	3.6 f_0	2	$0.2\lambda_g \times 0.15\lambda_g$	no
this work	1.51	43.7%	0.36	1.39 f_0–4.85 f_0	3	$0.063\lambda_g \times 0.50\lambda_g$	yes

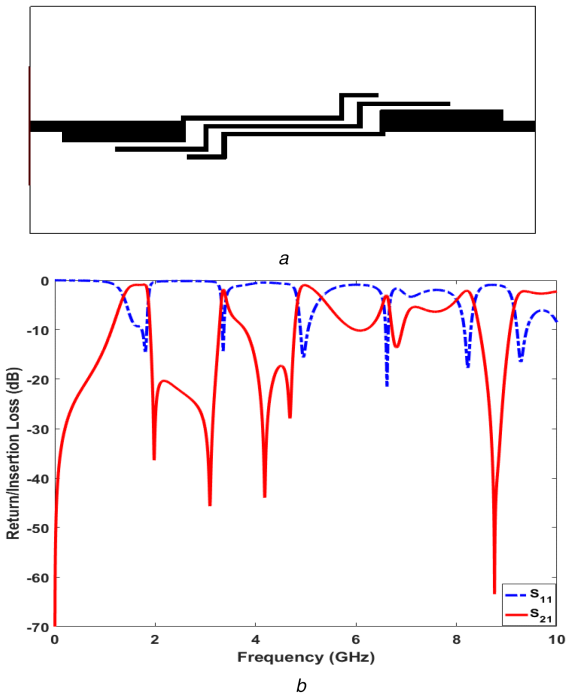

Fig. 10 *Three-pole bandpass*
(a) Three-pole structure of the proposed filter, ***(b)*** *S*-parameter performance for a three-pole structure

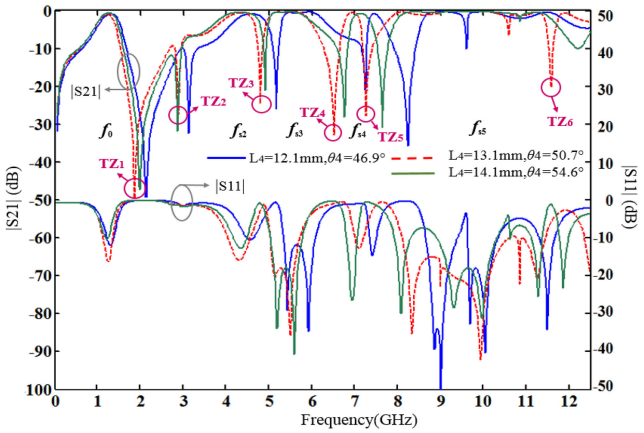

Fig. 11 *Variations of S_{11} and S_{21} versus different values of L_4*

values of L_4 are shown in Fig. 11. As shown in this figure, because of the multi-path coupling routing and TZs tuning method, six TZs (T_{Z1}–T_{Z6}) are generated, positioned between different pass bands to widen the pass BWs and improve the frequency selectivity. Moreover, the fifth operating band of more than 3.5 GHz−3 dB BW is generated, which is described as f_{s5} in the figure.

Fig. 12 plots the effect of L_4 on a quint-wideband-type SSMCL-ASIR. In (a), when L_4 varies from 10.1 to 16.1 mm, f_0 decreases while Q_{ex1}, normalised f_{s2} and Q_{ex2}/Q_{ex1} fluctuate. In (b), normalised f_{s3}, f_{s4} and f_{s5} increase slightly, and Q_{ex3}/Q_{ex1} fluctuates slightly. In contrast, Q_{ex4}/Q_{ex1} and Q_{ex5}/Q_{ex1} decrease dramatically

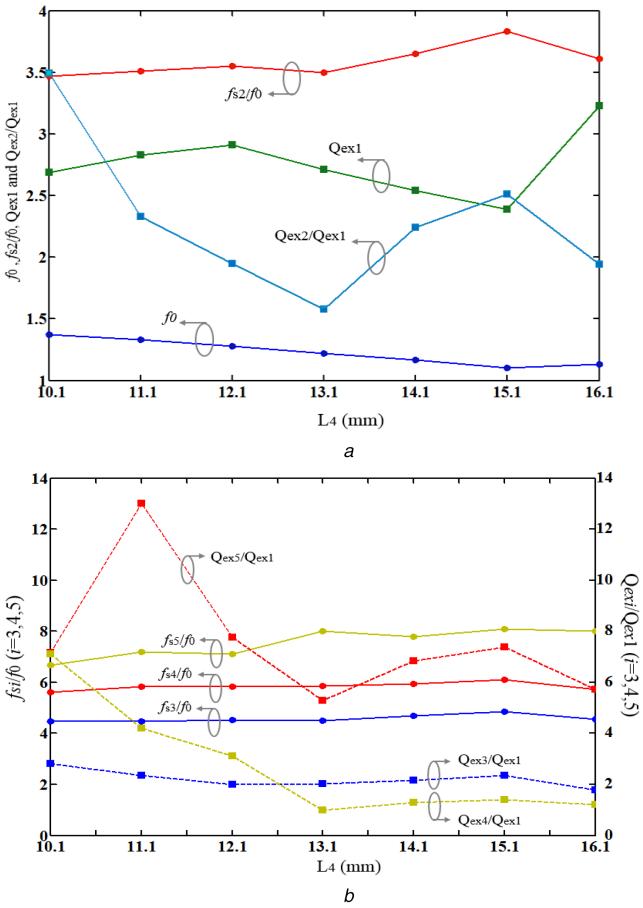

Fig. 12 *Effect of L_4 on quint-wideband-type SSMCL-ASIR*
(a) f_0, Q_{ex1}, f_{s2}/f_0 and Q_{ex2}/Q_{ex1} versus against L_4, ***(b)*** f_{si}/f_0 and Q_{exi}/Q_{ex1} ($i = 3$, 4, 5) versus against L_4

from 13 to 5.28 and from 7.1 to 1.2, respectively. Moreover, the notch of each Q_{exi}/Q_{ex1} ($i = 2$, 3, 4, 5) curve happens near $L_4 =$ 13.1 mm, which means that relatively second, third, fourth and fifth BWs of the proposed quint-band filter can be obtained with L_4~13.1 mm.

The design procedures for single- and quint-wideband-type SSMCL-ASIR BPFs can be summarised as follows:

i. Choose the suitable electrical length ratio α, thus setting the fundamental frequency f_0, and choose the characteristic impedance ratio K in the ASIR to realise improved insertion loss and return loss performance.
ii. Analyse the TZ generating requirement of the MCS added to the SS-ASIR structure and calculate the approximate TZ equations $S_{21} = 0$.
iii. According to the calculated results, tune the length of the MCS to meet $S_{21} = 0$ and make f_{zn} approach the resonant frequency f_{sm} to form a wide stopband for the single-wideband-type ASIR filter. The gap parameters S_1 and S_3 are also utilised and tuned to realise optimised results.

iv. Tune the length of the MCS to move f_{zn} away from f_{sm}, to enable a multi-band response with good isolation between operating bands for the multi-wideband-type ASIR filter.
v. Since of the non-wideband limitation of the coupling matrix, coupling coefficients are not important in this design, while external quality factor Q_{ex} can be discussed for performance optimisation, as mentioned above.

Simulated, measured results and a fabricated photograph of the quint-wideband-type SSMCL-ASIR filter are plotted in Fig. 13. Good agreement can be observed between the simulated and measured results, with discrepancies attributable to losses and fabrication errors.

It can be seen that quint widebands are realised with good in-band return loss performance. The first pass band ranges from 1.0 to 1.38 GHz with a CF of 1.19 GHz and BW of 380 MHz. The second pass band ranges from 3.96 to 4.62 GHz with CF 4.29 GHz and BW 660 MHz. The third pass band ranges from 5.0 to 5.86 GHz with CF 5.43 GHz and BW 860 MHz. The fourth pass band ranges from 6.82 to 7.12 GHz with CF 6.97 GHz and BW 300 MHz. The fifth pass band ranges from 7.96 to 11.84 GHz with CF 9.9 GHz and a large BW of 3.88 GHz. In addition, there are five TZs at 1.96, 2.98, 4.89, 6.68 and 7.58 GHz, which further enhance the frequency selectivity, illustrated in Fig. 13. The quint-wideband-type SSMCL-ASIR performance comparison with alternative quint-band BPFs is shown in Table 3.

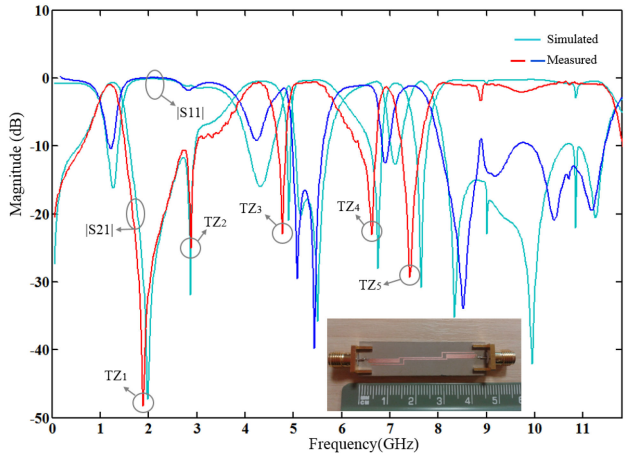

Fig. 13 *Simulated and measured results, and a photograph of a modified quint-wideband-type SSMCL-ASIR*

5 Tri-wideband band pass SS-ASIR filter design using asymmetric parallel uncoupled lines

An uncoupled section placed within conventional coupled lines is a useful way to achieve extra TZs close to existing zeros created by the conventional coupled lines. This way approach can also permit optimisation of the in-band performance of the original structure. As indicated in [23], the resonator unit can be further moved horizontally to the left or right so as to provide extra coupling between the coupling resonators. In this paper, the ASIR coupling structure in the vertical direction is further modified and an asymmetric parallel uncoupling microstrip line (APUML) structure is proposed. As shown in Fig. 14*a*, the two ASIR unit impedance line has an extra coupling with the low characteristic impedance line and this coupling length is S_t.

Moreover, there is a separation distance between two vertical symmetry axes of two parallel uncoupling microstrip lines, and this distance is controlled and influenced by the APUML relative distance parameters L_d, L_{d1} end and parameter S_t. The APUML's height and inner gap are L_m and W_m, respectively. The relative even-mode or odd-mode equivalent circuits of the proposed structure are shown in Fig. 14*b*. Z_{1e} or Z_{1o}, Z_{2e} or Z_{2o} and Z_{3e} or Z_{3o} are, respectively, the left, middle and right-coupled section's even-mode or odd-mode impedance. Z_2 and Z_3 or Z_4 and Z_5 have uncoupled sections in two coupled ASIRs, respectively.

Compared to traditional skew-coupled ASIR filters, a wider second pass band is achieved and the additional third operating band is generated by adopting the novel APUML. It is observed that this greatly improves the coupling strength between the two ASIRs.

Fig. 15 illustrates the influences of W_m and L_m on the response of the APUML-ASIR tri-band filter with different values of S_t. In (a), when W_m varies from 0.05 to 0.25 mm, f_0 decreases slightly and f_{s2}/f_0 increases slightly but neither are greatly influenced by varying S_t. Meanwhile, f_{s2}/f_0 does not change much but does less when S_t increases. In (b), when W_m varies from 0.05 to 0.25 mm, f_{z1}/f_0 decreases slightly while f_{z2}, $3/f_0$ hardly changes but when S_t becomes greater for a fixed W_m, $f_{z1,2,3}/f_0$ becomes less.

This means TZs can be controlled by W_m and S_t. In (c), when L_m varies from 1.7 to 2.9 mm, $f_{s1,2,3}/f_0$ decreases slightly. When S_t varies from 1 to 4 mm, f_0 and f_{s2}/f_0 do not vary but f_{s1}/f_0 decreases. In (d), when L_m varies from 1.7 to 2.9 mm, Q_{ex1} increases and $Q_{ex2,3}/Q_{ex1}$ decreases so that the fundamental BW becomes narrower. When S_t becomes greater, Q_{ex1} does not change and $Q_{ex2,3}/Q_{ex1}$ decreases. Compared to f_0, f_{s2}, f_{z1} and f_{z3}, the variation

Table 3 Performance comparison with the proposed quint-band BPF

Reference	CF, GHz	3 dB FBW, %	IL, dB	Size	Single/multi-band versatilities	Extra structure
[11]	0.6/0.9/1.2/1.5/1.8	5.8/5.2/5.8/8.2/8.0	2.8/2.9/2.9/2.6/2.3	$0.045\lambda_g \times 0.52\lambda_g$	no	via hole
[12]	0.63/1.33/2.03/2.74/3.45	28.8/9.4/2.7/5.3/5.5	0.47/1.14/1.8/1.39/ 1.26	$0.043\lambda_g \times 0.178\lambda_g$	no	via hole
[13]	1.5/2.5/3.5/4.5/5.8	4.5/4.5/3.6/4.5/2.7	1.5/1.8/0.9/1.2/ 2.5	$0.24\lambda_g \times 0.17\lambda_g$	no	multi-layer
this work	1.19/4.29/5.43/6.97/9.9	31.9/15.4/15.8/4.3/39.2	1.0/0.47/0.50/1.7/ 0.6	$0.05\lambda_g \times 0.40\lambda_g$	yes	none

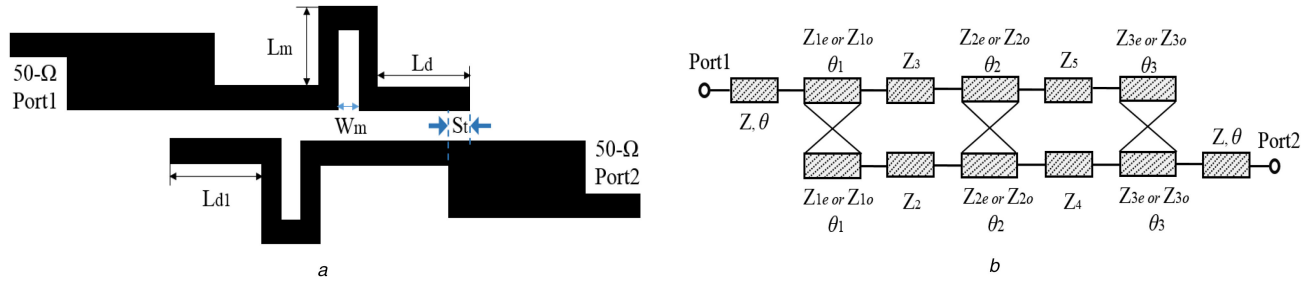

Fig. 14 *Schematic diagram of the SS-ASIR ASIR coupled pair with asymmetric parallel uncoupled meander sections*
(a) Schematic diagram, ***(b)*** Even-mode or odd-mode equivalent circuits

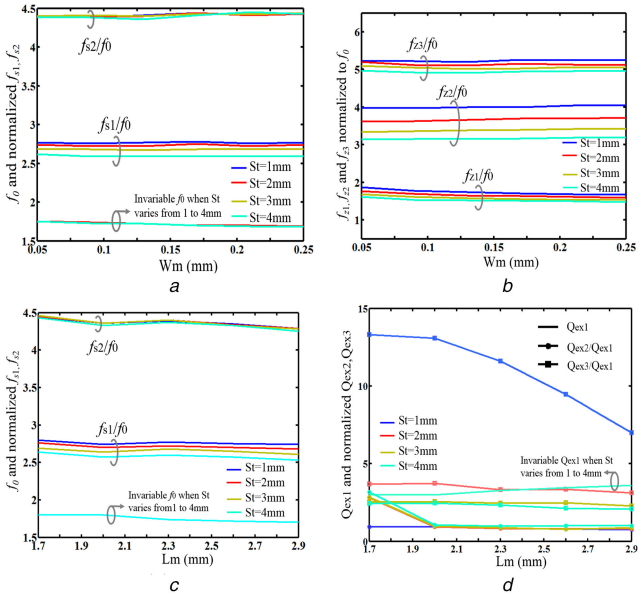

Fig. 15 *Influences of W_m and L_m on the response of the APUML-ASIR tri-band filter for variation of S_t*

(a) f_0 and normalised f_{si} (W_m varies), ***(b)*** Normalised f_{zi}, ***(c)*** f_0 and normalised f_{si}, (L_m varies), ***(d)*** Q_{ex1} and normalised Q_{exi}. When one parameter varies, the others remain unchanged

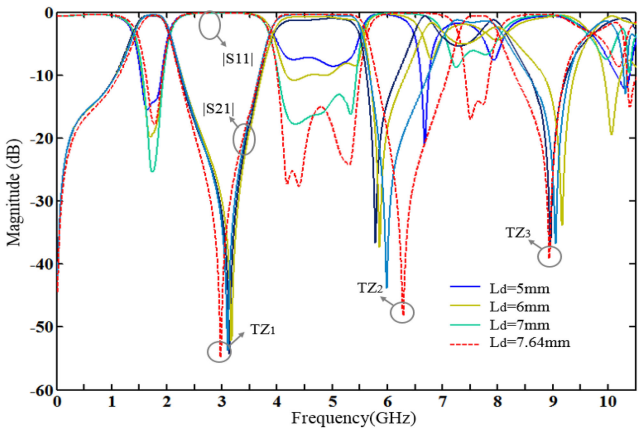

Fig. 16 *Impact of L_d impact on the frequency response of the SS-ASIR filter with APUMLs*

of S_t has a greater influence on the second pass band CF f_{s1}, the second TZ f_{z2} and the third pass BW.

Fig. 16 shows the effect of plot the reference location parameter L_d has on the frequency response of the proposed tri-band filter. It is noted that when L_d changes from 5 to 7.64 mm when L_{d1} is fixed at 8.1 mm, the second pass band return loss performance is enhanced greatly and its BW becomes wider, providing a wide second pass band of more than 3.5 GHz. At the same time, a third pass band is formed and its return loss as well as its insertion loss performance is improved considerably by varying L_d. Similar phenomenon can be observed when varying L_{d1} with fixed L_d. Therefore, L_d and L_{d1} are two important factors to tune and influence the coupling strength between two modified ASIRs and external quality factors.

The analysis of the APUML unit further helps to explain the formation of the second and third pass bands. The APUML topological structure and frequency response are plotted in Fig. 17: as seen in this figure, the APUML unit forms two wide pass bands between 4–6 and 6–8 GHz when L_{d1} changes from 9.1 to 7.1 mm.

This result proves the advantage of the APUML structure to optimise the in-band filter performance. As for out-of-band performance, the APUML unit generates four TZs at both sides of the pass bands, as plotted in Fig. 17. These four TZs can improve

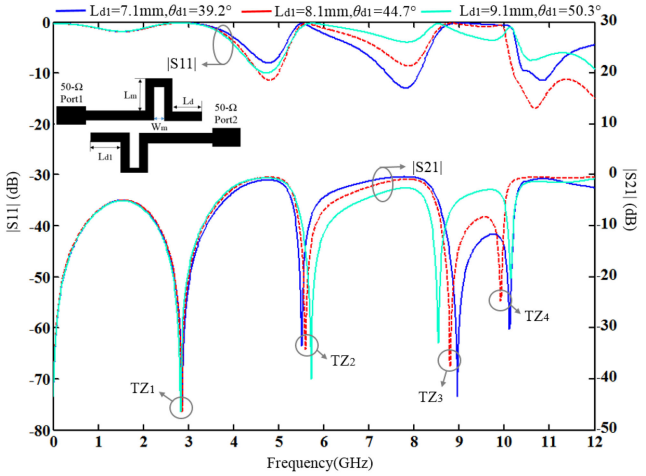

Fig. 17 *Analysis of the APUML structure*

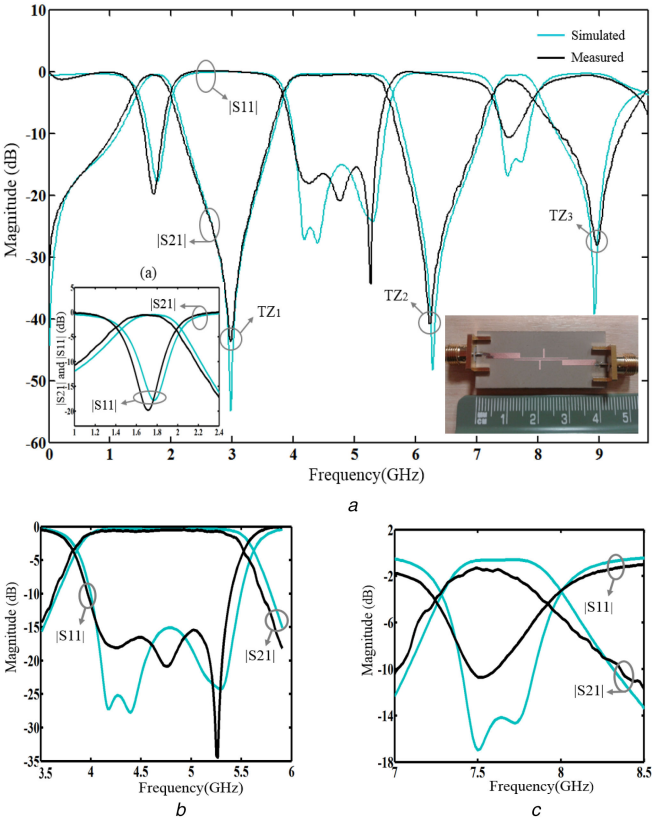

Fig. 18 *Simulated, measured results and a fabricated photograph of in SS-ASIRs with APUMLs*

(a) Narrowband view of the first passband, ***(b)*** Narrowband view of the second passband, ***(c)*** Narrowband view of the third passband

the isolation performance between the three pass bands, and the out-of-band suppression performance.

The simulated *S*-parameters, measured *S*-parameters and a fabricated photograph of the tri-wideband ASIR filter are shown in Fig. 18. Good agreement is observed between the simulated and measured results and the slight discrepancies are attributed to the loss and fabrication errors. It can be seen that triple widebands are realised with good in-band return loss performance. The first pass band ranges from 1.46 to 1.98 GHz with a CF of 1.72 GHz, BW 520 MHz and FBW 30.2%. It can be applied in the GPS (GPS: frequency band centred at 1.57 GHz), GSM communication (GSM: 1800 MHz) and UMTS (UMTS: 1710–1880 MHz etc.). The triple-wideband-type APUML-ASIR filter performance comparison with alternative tri-band BPFs is shown in Table 4.

The second pass band ranges from 3.90 to 5.54 GHz with CF 4.72 GHz, BW 1.64 GHz and FBW 34.7%. It can be applied in IEEE802.11a wireless local area network applications including

Table 4 Performance comparison with the proposed tri-band ASIR BPF

Reference	CF, GHz	3 dB FBW, %	IL, dB	$ISO_{1,2}$, $ISO_{2,3}$	Size	Extra structure
[12]	1.875/3.54/5.91	19.9/14/4.6	0.6/0.75/1.65	>27/>20	$0.206\lambda_g \times 0.086\lambda_g$	via hole
[14]	1.8/3.5/5.8	7/5/3.5	0.88/1.33/1.77	>40.4/>12.78	$0.108\lambda_g \times 0.521\lambda_g$	via hole
[15]	2/3.45/5.8	8.7/13.4/7.2	1.4/0.7/1.7	NA	$0.045\lambda_g \times 0.52\lambda_g$	via hole
[16]	2.4/3.5/5.45	11.6/6.7/17.8	1.1/1.2/1	<40/<40	$0.21\lambda_g \times 0.11\lambda_g$	via hole
this work	1.72/4.72/7.59	30.2/34.7/7.1	0.58/0.43/1.3	43.5/39.2	$0.09\lambda_g \times 0.51\lambda_g$	none

fifth-generation wireless fidelity. The third pass band, which ranges from 7.32 to 7.86 GHz with CF 7.59 GHz, BW 0.54 GHz and FBW 7.1%, can be applied in Earth-satellite satellite communication.

Moreover, good isolation is achieved between the three pass bands, to eliminate signal interference. Three TZs located at 3.02, 6.26 and 9.01 GHz are generated to enhance frequency selectivity, which can be seen in Fig. 18. Furthermore, it is significant that this design can be easily developed to handle and permit reconfigurability [24, 25] and can be easily integrated with antenna design [26], to create the so-called 'filtenna' [27].

6 Conclusion

Novel multi-standard single/tri/quint-wideband ASIR filters are proposed in this paper. By utilising a novel modified SS-ASIR coupled pair with MCSs, and placing TZs close to resonant frequencies, a single-wideband filter with good FBW, insertion loss and return loss performance is realised. By varying the lengths of MCSs, the stronger coupling between two resonators is realised and more TZs are generated, which are tuned to help in forming a quint operating wideband. With the help of APUML, a tri-wideband ASIR filter is realised with high fractional BW. These filters effectively cover several applications including GPS, GSM, UMTS, industrial, scientific and medical (ISM) and IEEE 802.11 a/b/g/n/ac, with controllable BWs. Furthermore, the proposed structures successfully realise ASIR filter applications in single/dual/triple/quadruple/quint-wideband fields with the advantage of higher versatility. Measured results agree well with simulated results and theoretical predictions. The good in-band and out-of-band behaviours, compact size and simple structure make the proposed filters very promising for applications in future multi-standard wireless communication.

7 Acknowledgments

This project has received funding from the European Union's Horizon 2020 research and innovation programme under Grant agreement H2020-MSCA-ITN-2016 SECRET-722424.

8 References

[1] Lin, S.-C., Deng, P.-H., Lin, Y.-S., *et al.*: 'Wide-stopband microstrip bandpass filters using dissimilar quarter-wavelength stepped-impedance resonators', *IEEE Trans. Microw. Theory Tech.*, 2006, **54**, (3), pp. 1011–1018

[2] Wang, H., Chu, Q.-X.: 'An EM-coupled triangular open-loop filter with transmission zeros very close to passband', *IEEE Microw. Wirel. Compon. Lett.*, 2009, **19**, (2), pp. 71–73

[3] Torabi, A., Forooraghi, K.: 'Miniature harmonic-suppressed microstrip bandpass filter using a triple-mode stub-loaded resonator and spur lines', *IEEE Microw. Wirel. Compon. Lett.*, 2011, **21**, (5), pp. 255–257

[4] Kim, C.H., Chang, K.: 'Wide-stopband bandpass filters using asymmetric stepped-impedance resonators', *IEEE Microw. Wirel. Compon. Lett.*, 2013, **23**, (2), pp. 69–71

[5] Al-Yasir, Y.I.A., Abd-Alhameed, R.A., Noras, J., *et al.*: 'Design of very compact combline band-pass filter for 5G applications'. Loughborough Antennas & Propagation Conf., Loughborough, UK, 2018

[6] Chen, C.F., Huang, T.Y., Wu, R.B.: 'Design of microstrip bandpass filters with multiorder spurious-mode suppression', *IEEE Trans. Microw. Theory Tech.*, 2005, **53**, (12), pp. 3788–3793

[7] Kuo, T.N., Lin, S.C., Wang, C.H., *et al.*: 'New coupling scheme for microstrip bandpass filters with quarter-wavelength resonators', *IEEE Trans. Microw. Theory Tech.*, 2008, **56**, (12), pp. 2930–2935

[8] Xu, J., Ji, Y.X., Miao, C., *et al.*: 'Compact single-/dual-wideband BPF using stubs loaded SIR (SsLSIR)', *IEEE Microw. Wirel. Compon. Lett.*, 2013, **23**, (7), pp. 338–340

[9] Fan, J., Zhan, D., Jin, C., *et al.*: 'Wideband microstrip bandpass filter based on quadruple mode ring resonator', *IEEE Microw. Wirel. Compon. Lett.*, 2012, **22**, (7), pp. 348–350

[10] Luo, X., Ma, J.-G., Li, E.-P.: 'Wideband bandpass filter with wide stopband using loaded BCMC stub and short-stub', *IEEE Microw. Wirel. Compon. Lett.*, 2011, **21**, (97), pp. 353–355

[11] Chen, C.F.: 'Design of a compact microstrip quint-band filter based on the tri-mode stub-loaded stepped-impedance resonators', *IEEE Microw. Wirel. Compon. Lett.*, 2012, **22**, (7), pp. 357–359

[12] Xu, J., Wu, W., Wei, G.: 'Compact multi-band bandpass filters with mixed electric and magnetic coupling using multiple-mode resonator', *IEEE Trans. Microw. Theory Tech.*, 2015, **63**, (12), pp. 3909–3919

[13] Hsu, K.W., Hung, W.C., Tu, W.H.: 'Compact quint-band microstrip bandpass filter using double-layered substrate'. IEEE MTT-S Int. Microwave Symp. Digest (IMS), Seattle, WA, 2013, pp. 1–4

[14] Zhang, S., Zhu, L.: 'Compact tri-band bandpass filter based on $\lambda/4$ resonators with U-folded coupled-line', *IEEE Microw. Wirel. Compon. Lett.*, 2013, **23**, (5), pp. 258–260

[15] Gao, L., Zhang, X.Y., Hu, B.J., *et al.*: 'Novel multi-stub loaded resonators and their applications to various bandpass filters', *IEEE Trans. Microw. Theory Tech.*, 2014, **62**, (5), pp. 1162–1172

[16] Gao, L., Zhang, X.Y., Xue, Q.: 'Compact tri-band bandpass filter using novel eight-mode resonator for 5G WiFi application', *IEEE Microw. Wirel. Compon. Lett.*, 2015, **25**, (10), pp. 660–662

[17] Kim, C.H., Chang, K.: 'Independently controllable dual-band bandpass filters using asymmetric stepped-impedance resonators', *IEEE Trans. Microw. Theory Tech.*, 2011, **59**, (12), pp. 3037–3047

[18] Wu, H.W., Yang, R.Y.: 'A new quad-band bandpass filter using asymmetric stepped impedance resonators', *IEEE Microw. Wirel. Compon. Lett.*, 2011, **21**, (4), pp. 203–205

[19] Chang, Y.C., Kao, C.H., Weng, M.H., *et al.*: 'Design of the compact wideband bandpass filter with low loss, high selectivity and wide stopband', *IEEE Microw. Wirel. Compon. Lett.*, 2008, **18**, (12), pp. 770–772

[20] Liu, H.W.: 'High-temperature superconducting bandpass filter using asymmetric stepped-impedance resonators with wide-stopband performance', *IEEE Trans. Appl. Supercond.*, 2015, **25**, (5), pp. 1–6

[21] Tang, C.W., You, S.F.: 'Miniaturised wide stopband rejected microstrip filter with coupled spur-lines', *Electron. Lett.*, 2006, **42**, (5), pp. 286–288

[22] Hong, J.S., Lancaster, M.J.: '*Microstrip filter for RF/microwave applications*' (Wiley, 2001)

[23] Azadegan, R., Sarabandi, K.: 'Miniature high-*Q* double-spiral slot-line resonator filters', *IEEE Trans. Microw. Theory Tech.*, 2004, **52**, (5), pp. 1548–1557

[24] Yuceer, M.: 'A reconfigurable microwave combline filter', *IEEE Trans. Circuits Syst. II, Express Briefs*, 2016, **63**, (1), pp. 84–88

[25] Al-Yasir, Y.I.A., Ojaroudi Parchin, N., Abd-Alhameed, R., *et al.*: 'Recent progress in the design of 4G/5G reconfigurable filters', *Electronics. (Basel)*, 2019, **8**, (1), pp. 1–17

[26] Al-Yasir, Y.I.A., Abdullah, A., Mohammed, H., *et al.*: 'Design of frequency-reconfigurable multiband compact antenna using two PIN diodes for WLAN/WiMAX applications', *IET Microwaves Antennas Propag.*, 2017, **11**, (8), pp. 1098–1105

[27] Atallah, H., Abdul Rahman, A., Yoshitomi, K., *et al.*: 'Compact frequency reconfigurable filtennas using varactor loaded *t*-shaped and *h*-shaped resonators for cognitive radio applications', *IET Microwaves Antennas Propag.*, 2016, **10**, (9), pp. 991–1001